Journal of Cultural Heritage 15 (2014) 266–274

Available online at
SciVerse ScienceDirect
www.sciencedirect.com

Elsevier Masson France
EM|consulte
www.em-consulte.com/en

Original article

Historical pigments characterisation by quantitative X-ray fluorescence

Dorotea Fontana[a,b,*], Maria Francesca Alberghina[a,b], Rosita Barraco[a,b], Salvatore Basile[c], Luigi Tranchina[b], Maria Brai[a,b], Anna Gueli[d], Sebastiano Olindo Troja[d]

[a] *Dipartimento di Fisica e Chimica, Università degli Studi di Palermo, Viale delle Scienze, Edificio 18, 90128 Palermo, Italy*
[b] *Laboratorio di Fisica e Tecnologie Relative–UniNetLab, Università degli Studi di Palermo, Viale delle Scienze, Edificio 18, 90128 Palermo, Italy*
[c] *Dipartimento Energia, Ingegneria dell'Informazione e Modelli Matematici, Università degli Studi di Palermo, Viale delle Scienze, Edificio 9, 90128 Palermo, Italy*
[d] *PH3DRA Laboratories (PHysics for Dating Diagnostics Dosimetry Research and Applications), Dipartimento di Fisica e Astronomia, Università degli Studi di Catania & INFN Sezione di Catania, Via Santa Sofia 64, 95123 Catania, Italy*

ARTICLE INFO

Article history:
Received 10 October 2012
Accepted 2 July 2013
Available online 29 July 2013

Keywords:
Pigments
Mixtures
Quantitative analysis
X-ray fluorescence
Cultural heritage

ABSTRACT

Most of the historical paints are mainly constituted by inorganic pigments, either pure or mixed, spread on the surfaces using different binding agents. The knowledge of the exact amount of different constituents of the paint, as well as of the mixing and pictorial techniques, is crucial for a careful program of conservation of polychrome works. Moreover, since the availability of these pigments has been changing through the centuries, their identification and chemical characterisation is useful to acquire or deepen information about the artist and his/her work. This information can also be useful for authentication purposes through relative dating because the identification of one pigment respect to another one can be used as a *terminus post quem* or *ante quem* the artwork was realized. In this work, X-ray fluorescence data from historical pigments, both pure and mixed, will be presented, in order to obtain quantitative information on the samples and to extract calibration curves to the aim of evaluating the pigment concentration in unknown mixtures.

© 2013 Elsevier Masson SAS. All rights reserved.

1. Research aim

This work is focused on the chemical characterization and quantitative analysis of binary mixtures obtained by mixing three historical pigments: cinnabar, lapis lazuli and lead-tin yellow.

They were analysed both in pure and mixed form, by varying their weight percentage, in order to produce binary mixtures to be investigated by means of a portable XRF spectrometer in order to carry out qualitative and quantitative analyses of the two pigments constituent the mixture.

This experimental approach allows calculating the weight percentage of the single component, on an unknown (for the analyst) mixture, composed by two known pigment, by inverse prediction on the calibration curve.

Final aim is to apply, in the future, these calibration curves to a real study case, in order to determine the quantity of pigment used to prepare the paint under analysis.

2. Introduction

The characterization of the materials constituting a work of art is the main issue for obtaining fundamental information necessary in planning an appropriate conservation procedure in the field of Cultural Heritage (CH). The knowledge of the chemical composition of the works of art, indeed, offers an insight on the realization techniques used by the artists, on the presence of forgeries and retouches, on the degradation processes affecting the CH and on the compatibility of the materials to be used for the conservation. In this context, the identification and chemical characterization of pigments also play a relevant role, in order to answer technical and historical questions and to track the original appearance of the works of art [1].

The pigments have always been part of the colour palette of the artists, thanks to their high colouring power, availability, stability and persistence over time [2]. The different historical epochs have seen the introduction of new pigments either in their pure form or in special mixtures so expanding the palette of the available

* Corresponding author. Dipartimento di Fisica e Chimica, Università degli Studi di Palermo, Viale delle Scienze, Edificio 18, 90128 Palermo, Italy.
Tel.: +39 091 23899149.
E-mail addresses: dorotea.fontana@unipa.it (D. Fontana), maria.alberghina@unipa.it (M.F. Alberghina), rosita.barraco@unipa.it (R. Barraco), salvatore.basile@unipa.it (S. Basile), luigi.tranchina@unipa.it (L. Tranchina), maria.brai@unipa.it (M. Brai), anna.gueli@ct.infn.it (A. Gueli), olindo.troja@ct.infn.it (S.O. Troja).

1296-2074/$ – see front matter © 2013 Elsevier Masson SAS. All rights reserved.
http://dx.doi.org/10.1016/j.culher.2013.07.001

Table 1
Survey of the analysed inorganic pigments and some of their characteristics.

Colour	Pigment	ID Kremer	Chemical formula	Origin	Historical information
Red	*Cinnabar*	*10620*	*HgS*	Inorganic natural mineral	Known by the ancient Chineses, Egyptians, Greeks and Romans. Used until mid of 20th century.
Yellow	*Lead-Tin Yellow*	*10100*	Pb_2SnO_4	Inorganic synthetic Mineral	Known by the ancient Egyptians and the Assyrians.
Blue	*Lapis Lazuli*	*10520*	$3Na_2O{*}3Al_2{*}6SiO_2{*}2Na_2S$	Inorganic natural Mineral	Since antiquity used in Arabia, China, in Persia

colours. The study of the pigment features has been topic of many paper focused on pigment identification, characterization and dating [3–5]. In particular, chemical characterization by X-ray fluorescence (XRF) technique has been very important in the study of works of art, such as icons, frescoes, sculptures, ceramics, murals, porcelain, paper and other materials [6].

The need for reliable chemical and physical techniques allowing non-destructive and *in situ* investigations is increasing [7–9]. These features are guaranteed by the portable XRF spectrometers, widely used in the CH field [10–16].

Nevertheless, if the qualitative analysis is now widely established and widespread, there are still open questions concerning the quantitative analysis especially when complex matrices are investigated. This is the case of pictorial mixtures, where the pigments can be inhomogeneously distributed and mixed with variable concentrations.

In these samples, the absorption of X-rays through different constituent elements will result in a modification of the detected intensity due to the mixture density, and to the shielding effect due to the heavier component.

Starting from that point of view, Raman, XRD and XRF measurements were carried out to characterize the pigments used to prepare binary mixtures.

Finally, this paper aims to quantitatively analyse binary mixtures of known pigments by portable XRF equipments. Moreover, the elemental peak intensity behaviours of XRF measurement have been evaluated as function of samples densities to obtain an analytical law describing the phenomenon.

The studied pigments include three hues of the most widely employed pigments, namely cinnabar (red: R), lapis lazuli (blue: B), and lead-tin yellow (yellow: Y). Mixtures have been obtained by mixing two pigments and varying their weight percentage composition. They were characterized by XRF on the basis of their characteristic chemical elements widely used for the *in situ* characterization of pigments [17–25].

3. Experimental

3.1. Samples

In order to gather information eventually useful for the database implementation, laboratory specimens have been prepared using some pigments widely used for historic works of art: cinnabar, lapis lazuli and lead-tin yellow.

Cinnabar, a mineral compound of mercuric sulphide (HgS), is a very opaque bright, pure red, which works well in oil [26,27].

The pigment has been used since ancient times and has been found in China, Egypt, Assyria, Greece, Rome, Judaea, Mexico, and Peru. Since the time of *Albertus Magnus* (13th century), this pigment has also been obtained from mercury and sulphur by various wet or dry methods; it was named vermilion, whose properties are practically the same as the natural cinnabar. Due to its toxicity (mainly caused by mercury), it was eventually substituted by cadmium red in the first decades of the 20th century, losing its practical importance [28,29].

Lapis lazuli is a rock, containing small and variable amounts of calcite ($CaCO_3$) and pyrite (FeS_2). It is mainly composed by the cubic mineral lazurite [$Na_3Ca(Al_3Si_3O_{12})S$]. Lapis lazuli use is widely spread through different epochs. It is mainly found in Afghanistan, and in Tibet, but also in Spain and Chile [30]. The earliest findings in art have been found in Sumerian mosaics from the third millennium B.C. Other examples were discovered in the treasury of Rameses II.

Lead-tin yellow is one of the earliest pigments studied in both glass colouring and painting [31] and it continues to attract scientific interest nowadays. However, relatively little is known about the actual manufacturing of lead-tin yellow pigment in ancient times [32]. Well-known in medieval epoch in Italy, it was discovered in the 13th century and used through the 18th century. The bright yellow in old-master paintings was erroneously described as Naples yellow (lead antimoniate) [26]. Things were made clear when the lead-tin yellow was identified by spectral analysis as lead ortho-stannate (lead-tin yellow type I or type II) [26–33].

All the analysed samples were pigment powders compressed by a 1.8 Tons pressure into tablets of 1.2 cm diameter and 0.2 cm thick. They refer to the well-known Kremer's collection of artist's pigments. Name, corresponding catalogue number, chemical composition, origin and historical information of each sample are reported in Table 1. The densities of cinnabar, lead-tin yellow and lapis lazuli are 8.1, 6.6 and 2.4 g cm^{-3}, respectively [34].

The prepared binary mixtures represent the triad of Itten secondary colours, i.e. violet, green and orange, obtained by mixing the primary ones R(ed) and B(lue), Y(ellow) and B(lue), Y(ellow) and R(ed) respectively [35].

The mixtures were made by varying, in 10% weight steps, the percentages of the component pigments obtaining a 500 mg mixture. The weight measurements have been carried out with an analytical balance (62 g × 0.1 mg).

The density $D_{I,J}$ of each mixture has been calculated from the densities D_I and D_J and mass percentages p_I and p_J of the pure pigments according to the following equation:

$$D_{I,J} = \frac{p_I + p_J}{\frac{p_I}{D_I} + \frac{p_J}{D_J}} \quad (1)$$

Further tests have been carried out in order to check and validate the procedure, performing inverse predictions on fitting or calibration curves.

3.2. Analytical techniques

3.2.1. Micro-Raman spectroscopy

Raman micro-spectroscopy was undertaken using an instrumental apparatus equipped with a micro sampling system which uses the microscope objective to focus the laser beam on the sample and to collect the scattered light. This configuration allows to analyse very small portions of sample, reaching spatial resolution values of the order of few microns. The optical source operating at 785 nm whose beam is focused, through a Olympus BX40 confocal microscope, either with 10× or 50× objective lenses. Interferences, caused by the fluorescence background, were minimised by the use of the near-infrared laser. The Raman scattered light is collected by a TRIAX 320 spectrometer from Horiba Jobin-Yvon characterized from 1800 grooves mm^{-1} dispersive grating and a spectral resolution of 3 cm^{-1}. The dispersed spectrum is sent to a charge-coupled

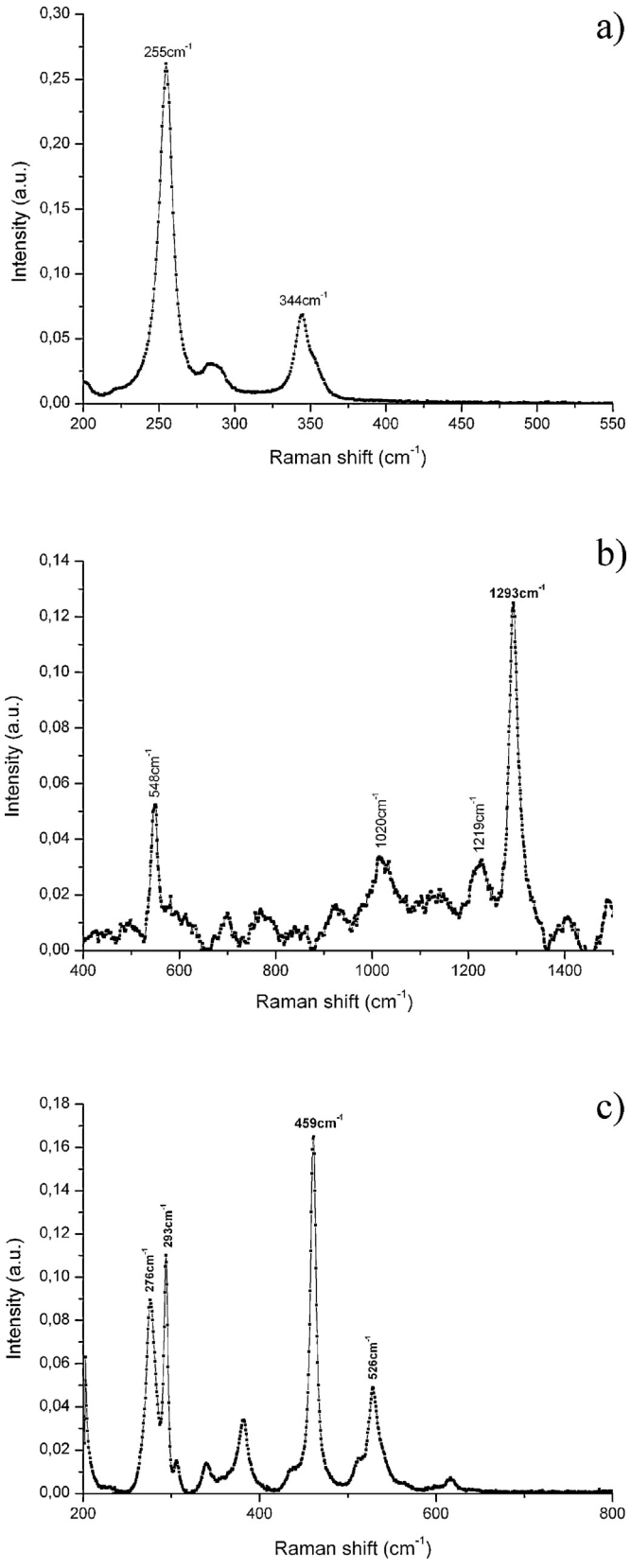

Fig. 1. Raman spectra of the pure pigments, the characteristic peaks are labeled: (a) cinnabar; (b) lapis lazuli; (c) lead-tin yellow.

device detector (CCD: 1024 × 128), and then processed, amplified and digitalised by the CCD control unit (Symphony).

The Raman measurements were obtained on powder samples of the pure pigments using the 50× objective lens. All measurements

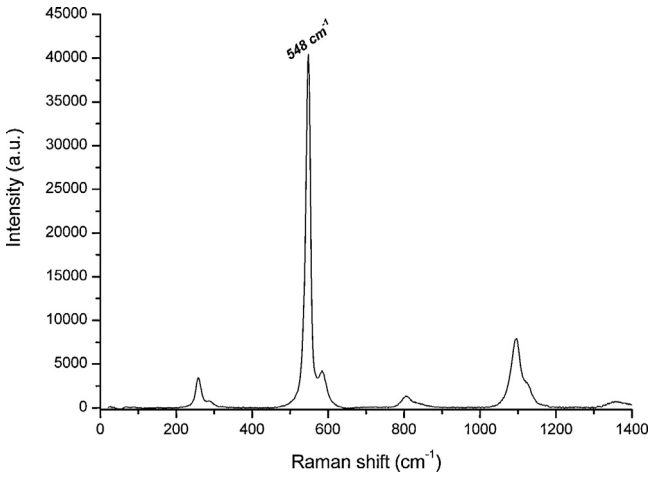

Fig. 2. Raman spectrum of lapis lazuli acquired using the 514 nm excitation wavelength.

were acquired in the spectral range 200–1200 cm^{-1} with collection times varying in the range from 2 to 100 seconds and accumulation of two scans to provide a suitable signal-to-noise ratio (SNR) enhancement. Spectra were calibrated in intensity through the acquisition and subsequent processing of the standard NIST SRM2241 spectrum (NIST-Standard Reference Material) related to the laser intensity of 785 nm.

3.2.2. X-ray fluorescence

A portable XRF system, namely the ArtTAX 400 spectrometer from Bruker AXS, was used to acquire XRF spectra. It is equipped with a Mo (K_α = 17.5 keV) low-power excitation tube (with a 100 μm thick beryllium window), enclosed by a safety radiation shield. A filter disk system, put before the X-ray beam placed between the X-ray tube and the sample, can be used in order to attenuate the Bremsstrahlung radiation and to reduce the diffracted component of the X-ray beam. A pinhole system in the X-ray source provides a collimated beam on the sample making the instrument suitable to perform spatially resolved multi-elemental analysis on three-dimensional structures. The detector is an XFlash 1001 (a Peltier cooled silicon drift detector) with high speed, low noise electronics, and a FWHM energy resolution below 145 eV at the Mn K_α energy (5.9 keV) with an active area of 5 mm^2 and an 8 μm beryllium window. The detection head contains the detector and the X-ray tube, fixed on a movable tripod allowing independent vertical and horizontal movement, and its power supply. The mobile XRF moving head includes also a microcamera to visualise the positioning of the incident beam on the sample. Helium flux system, reducing the photoelectric absorption of the sample characteristic X-rays by the air molecules, allows the detection of light elements. In particular, this XRF equipment allows the detection of chemical elements with atomic number Z above 11 (i.e. Na) [36].

The geometry between primary beam, sample, and detector is fixed at 0°/40° relative to the perpendicular of the sample surface [36]. Measurement setup was as follows: tube voltage 25 and 40 kV; current 1300 and 700 μA; acquisition time 300 s; no filter disk between the X-ray tube and the sample; He flow rate 1.6 L min^{-1}, lateral resolution 0.65 mm. The setup parameters were selected such to have a good spectral signal and to optimise the SNR. The outcomes of three independent measurements were averaged, in order to improve the statistical significance.

The element calibration curves have been built by considering the related XFR intensity for each known mixture. In order to reverse estimate the pigments concentration of the unknown (for analyst) mixtures, out of fixed 10% step samples have been made.

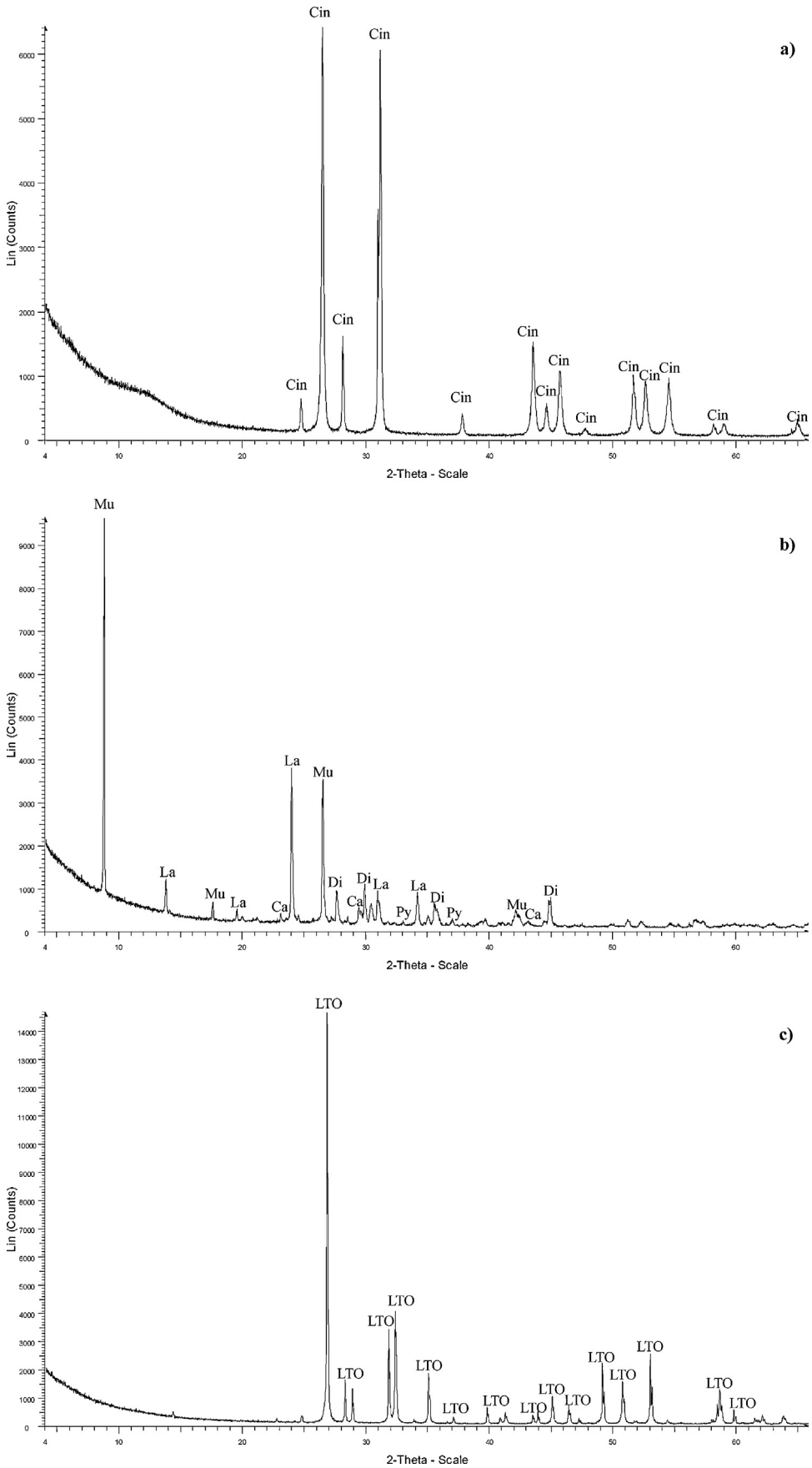

Fig. 3. XRD spectra: (a) cinnabar; (b) lapis lazuli and (c) lead-tin yellow. Mineralogical phases are reported: Cin: cinnabar; LTO: lead-tin oxide; La: lazurite; Mu: muscovite; Di: diopside; Ca: calcite; Py: pyrite.

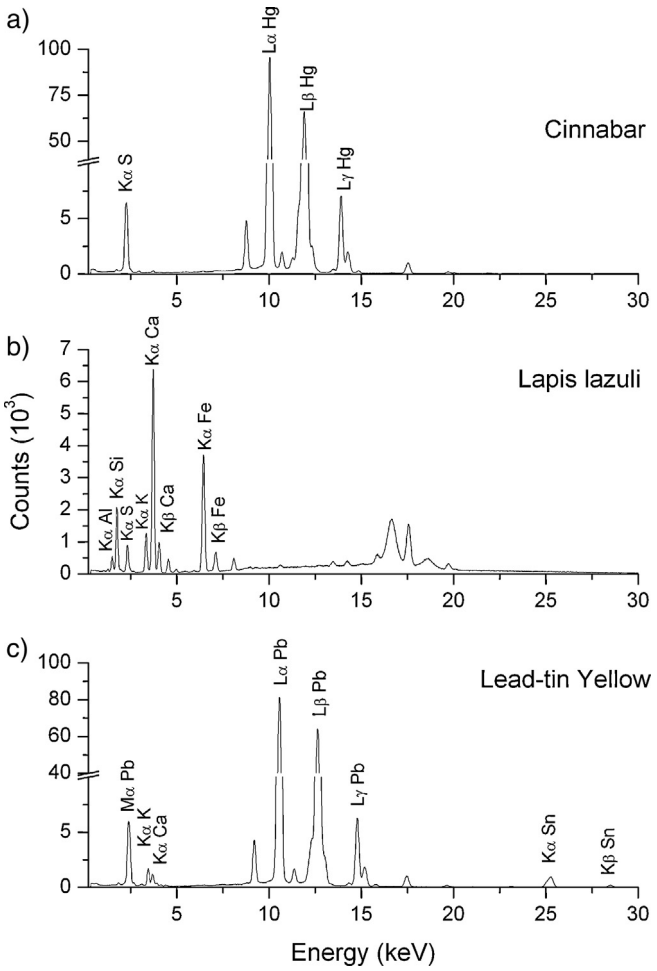

Fig. 4. XRF spectra: (a) cinnabar; (b) lapis lazuli; (c) lead-tin yellow; from top to bottom.

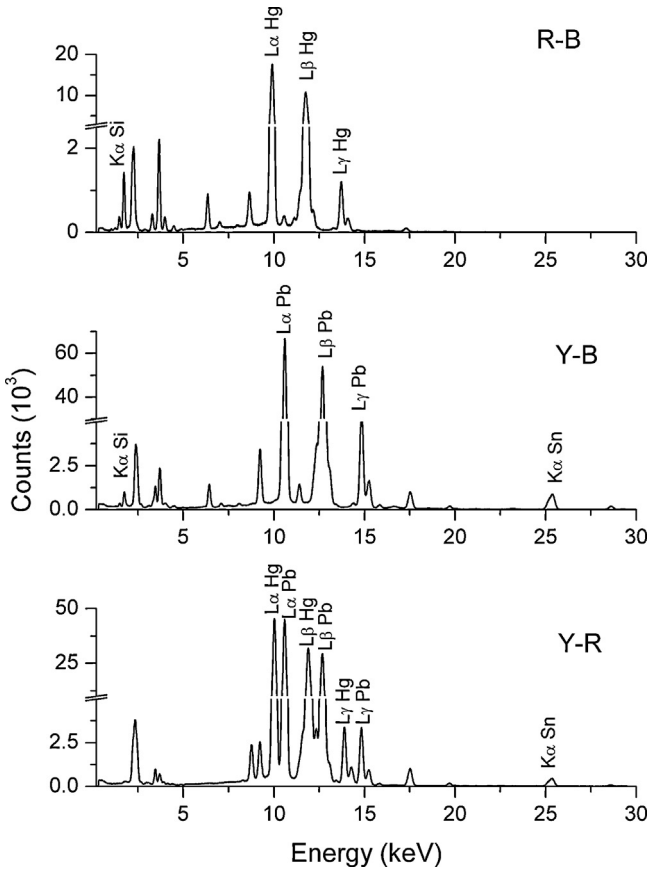

Fig. 5. XRF spectra of the 50% mixtures, from top to bottom: cinnabar and lapis lazuli (R-B), lead-tin yellow and lapis lazuli (Y-B), and lead-tin yellow and cinnabar (Y-R).

4. Results and discussion

Micro-Raman investigations have been carried out in order to characterize the pure pigments. Fig. 1 shows the Raman spectra of the pure pigments, with baseline correction and intensity calibrated according to the NIST standard. On the basis of the collected vibrational data, it is possible to conclude the all the spectra of the investigated pigments exhibit the characteristics peaks [37], which allow their identification. In particular, the cinnabar exhibits peaks at 255 and 344 cm^{-1} [38,39], lead-tin yellow (type I) shows marker bands centred at 276, 294 and 459 cm^{-1} [38], and lapis lazuli presents the band at 548 cm^{-1} [40,41], typical of lazurite, and a band at 1293 cm^{-1} not imputable to lazurite; to verify the purity of lapis lazuli, the same sample was analyzed using 514 nm laser line. The spectrum, reported in Fig. 2, show only the main band of lazurite demonstrating that the sample is characterized by the presence of this mineral phase.

To better characterize the lapis lazuli sample and to evaluate the mineralogical phases present into each pigment, XRD measurements were carried out using a Bruker D8 ADVANCE XR diffractometer, managed through the software EVA DIFFRAC PLUS.

The spectra, reported in Fig. 3, show the mineralogical composition of pigments. In particular, the red pigment (Fig. 3a) is composed only by cinnabar (HgS), the yellow one (Fig. 3c) presents only the characteristic peaks of lead-tin oxide (Pb_2SnO_4) whereas the blue pigment shows the presents of different minerals. The spectrum of lapis lazuli (Fig. 3b) displays peaks of: lazurite, muscovite, diopside, calcite and pyrite.

None of this minerals presents a band at 1293 cm^{-1}, further studies will be aimed to better understand its origin.

On the other hand, XRF spectra of the three pure pigments (Fig. 4) show, beside the characteristic chemical elements, also some impurities due to both the mineralogical origin and/or the production procedures.

Specifically, the cinnabar spectrum is dominated by the Hg *L*-lines, with also Si traces (not labelled in the spectrum). The elemental composition of lapis lazuli yields a more complex spectrum. It shows Al, Si and S *K*-lines and a weak (due to instrumental limitations for low *Z* elements) contribution from the Na *K*-lines, that are all characteristic elements of lazurite mineral (the main component of this pigment). The presence of Mg, K, Ca and Fe is related to the other typical mineralogical phases of the lapis lazuli as confirmed by the XRD analysis carried out on this samples. Finally, the lead-tin yellow spectrum is characterized by the Pb *L*-lines and Sn *K*-lines, with traces of K and Ca.

It is worth pointing out that, in this work, the S K_α line is not taken into account because it is too close to the *L*-lines of Mo and Hg and also to the Pb *M*-lines.

Spectra for R-B, Y-B and Y-R mixtures, obtained as discussed above, have been collected and analysed. By way of illustration, Fig. 5 shows, from top to bottom, XRF spectra for R-B, Y-B and Y-R 50% mixtures. All the characteristic elements peaks of primary pigments are present in the spectra with peak areas proportional to their relative concentration.

In order to build fitting and calibration curves, to be used to obtain by inverse prediction the concentration of the two pigments composing the mixture, net area values for selected peaks

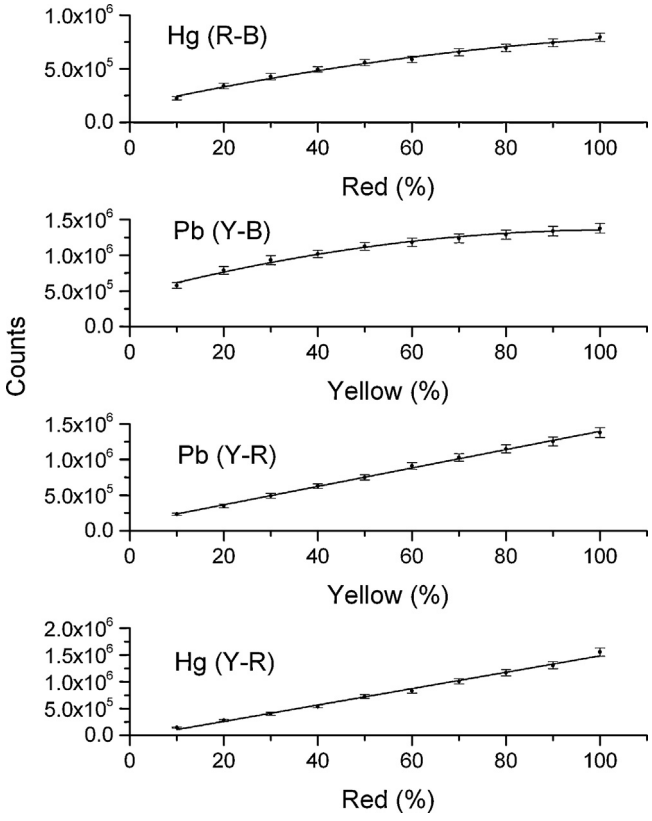

Fig. 6. Experimental net peak areas *vs.* pigment weight fraction and fitting curves. Error bars are also shown. From top to bottom: Hg in R-B *vs.* R%; Pb in Y-B *vs.* Y%; Pb in Y-R *vs.* Y%; Hg in Y-R *vs.* R%. See Table 2 for numerical details.

of pigments characteristic elements have been plotted *vs.* pigment concentration (weight %).

Only chemical elements directly related to the presence of the three main pigments, and having statistically significant peak counts, have been used for fitting. These elements are: Hg for cinnabar, Si for lapis lazuli and Pb and Sn for lead-tin yellow. Table 2 reports a summary of the fitting curves results.

It is well known that, the quantitative XRF analysis is based on the fundamental requirement of microscopic homogeneity of sample composition through the probed thickness. Such homogeneity must hold on distances much smaller than the average length travelled by characteristic X-rays [42]. The XRF signal strongly depends

Table 2
Numerical results for fitting of peak net areas vs. pigment concentrations. The second column lists the model along with the R^2 values. The last two columns list the expected weight percentages of pigments in the test binary mixtures (reference values %) along with the values obtained by inverse prediction. In the case of a linear regression model, the concentration and their ≅95% confidence ranges are also shown.

Mixture (element)	Model (R^2)	Reference value (%)	Calculated value (%)
R-B (Hg)	Quadratic (0.992)	R 75	R 75.7
B-Y (Pb)	Quadratic (0.989)	Y 85	Y 83.9
B-Y (Si)	Quadratic (0.998)	B 15	B 18.4
R-Y (Pb)	Linear (0.998)	Y 25	Y 24.3 (21.0 – 27.6)
R-Y (Hg)	Linear (0.994)	R 75	R 73.3 (67.5 – 79.1)
R-Y (Sn)	Linear (0.997)	Y 25	Y 24.8 (20.4 – 29.1)

on the weight fraction of the elements constituting the samples [10,43]. This means that the densities of samples in R-B and Y-B mixtures, obtained by mixing pigments with different relative densities, affect the XRF signal, which will be then strongly dependent on the relative percentage of the two pigments in the mixing. This circumstance will be less important in mixtures composed by pigments characterised by comparable densities (e.g. Y-R).

What stated above is evident in the calibration and fitting curves shown in Fig. 6. In this figure, net areas for Hg L_α line in the R-B mixture *vs.* R% concentration, and Pb L_α line in the Y-B mixture *vs.* Y% concentration (the two top plots in Fig. 6) have been fitted by a second order polynomial equation. This non-linearity, with a decreasing slope of the curve, can be explained by the fact that the density of the sample will strongly increase with the heavy pigment (R or Y) percentage. The opposite behaviour, with an increasing slope, would be obviously obtained by plotting the XRF signal *vs.* the light pigment concentration (*e.g.* Si K_α peak area *vs.* B percentage in the Y-B mixture, Table 2). In the case of Y-R mixtures, the two pigments have comparable densities, the peak intensity will not be influenced by density of the mixtures, so leading to a linear behaviour in calibration curves ($R^2 > 0.99$). The same behaviour is obtained for the Sn K_α line *vs.* Y% (not shown in Fig. 6).

XRF data for the different mixtures have been analysed in detail in order to get insights on the mixture density dependence.

The densities value of the three pure pigments are: 8.1 g cm^{-3} for cinnabar, 6.6 g cm^{-3} for lead-tin yellow and 2.75 g cm^{-3} for lapis lazuli. Only the last one, the lapis lazuli, has a density value higher than one declared by Kremer. Indeed, the XRD analysis carried out in order to better characterize the chemical composition and the mineralogical phases of the three pure pigments shows that the red and yellow pigment presents only the mineralogical phases

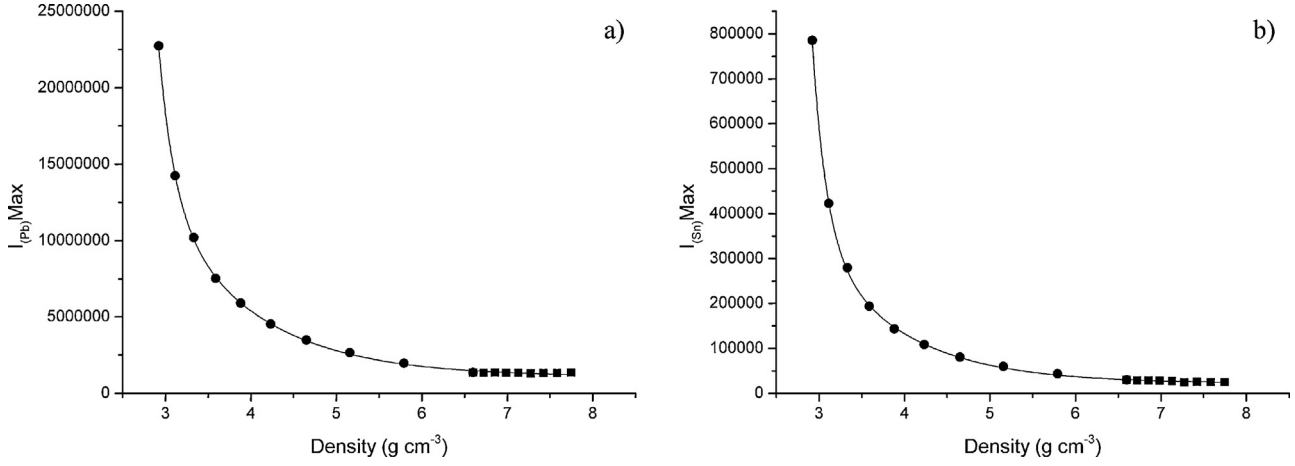

Fig. 7. I_{max} values and fitting curves according eq. (3) in the density range of the Y-B and Y-R mixtures, i.e. from 2.58 g cm^{-3} in the 10% Y–90% B mixture up to 7.92 g cm^{-3} in the 10% Y–90% R mixture, for: (a) Pb, fitting curve with $R^2 = 0.999$ and (b) Sn, fitting curve with $R^2 = 0.999$.

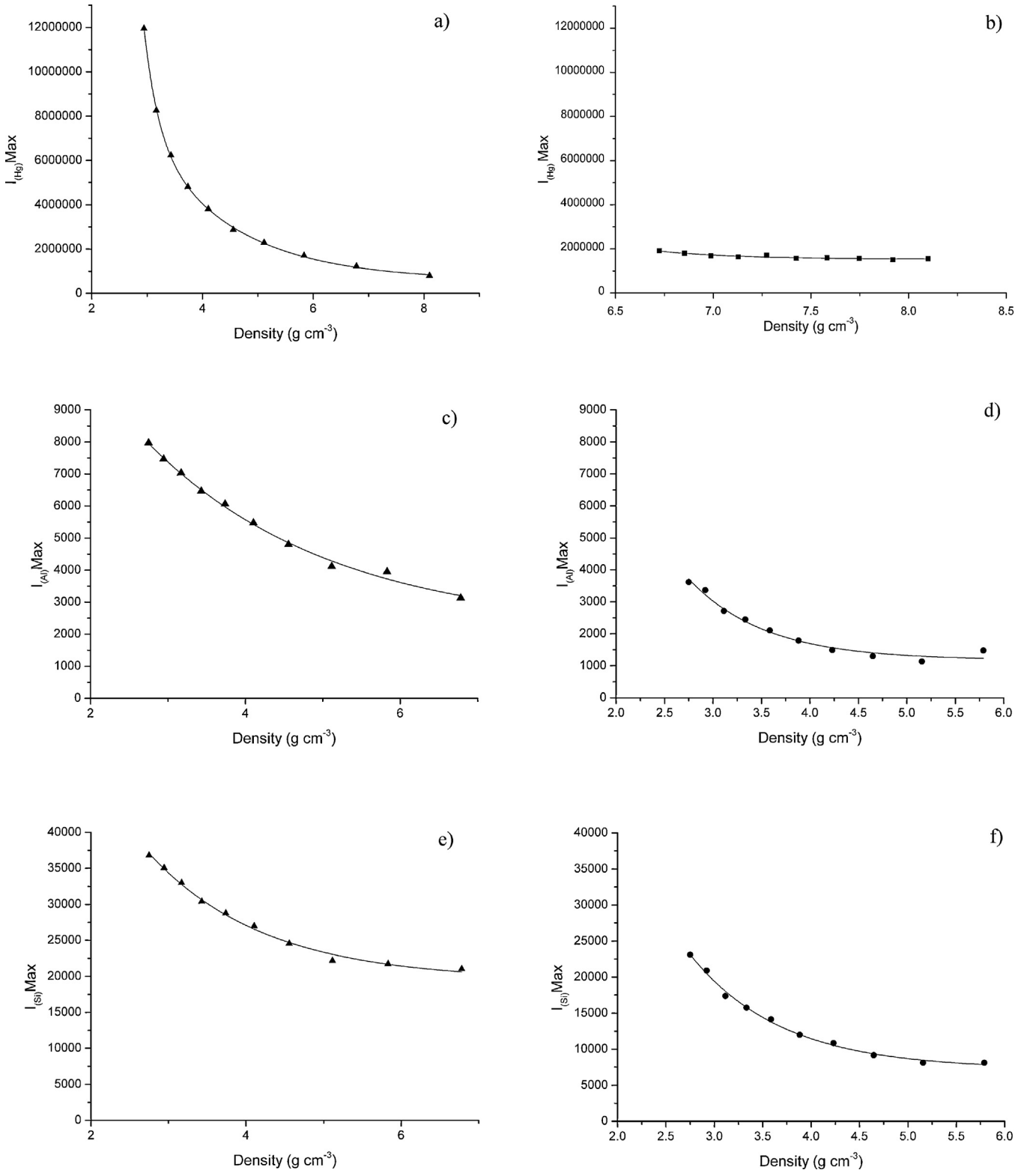

Fig. 8. I_{max} values and fitting curves according eq. (3) for: Hg (a) in R-B mixtures, fitting curve with $R^2 = 0.999$; (b) in R-Y mixtures, fitting curve with $R^2 = 0.999$; Al (c) in B-R mixtures, fitting curve with $R^2 = 0.993$ and (d) in B-Y mixtures, fitting curve with $R^2 = 0.993$; Si (e) in B-R mixtures, fitting curve with $R^2 = 0.994$ and (f) in B-Y mixtures, fitting curve with $R^2 = 0.995$. Measurement parameters used for the XRF acquisitions: 25 kV and 1300 μA for (a), (c) and (e) spectra; 40 kV and 700 μA for (b), (d) and (f) spectra.

declared by Kremer (cinnabar and lead-tin oxide respectively), on the contrary, the lapis lazuli matrix appear more complex, characterized by the presence of various mineral phases: lazurite, muscovite, diopside, calcite and pyrite with weight percentage of 40, 31, 17, 8 and 4% respectively; hence the density value of this pigment was calculated by eq. (1), using the weight % of the different minerals present.

In particular, we define the maximum value I_{max} of XRF intensity which can obtained from a chemical element in an hypothetical mixture, having the density of the measured mixture and the

molar fraction x of the element taken into account in the pure pigment. For example, in the case of Pb, I_{max} can be then calculated as follows:

$$I_{Pb(\max)} = \frac{I_{Pb(R+Y)} x_{Pb(Y)}}{x_{Pb(R+Y)}} \quad (2)$$

Thus, the I_{max} behaviour can be considered as an indicator of how the variation of the mixture density affects the XRF response of a particular chemical element. In other words: if there is no correlation between density and XRF response, I_{max} should remain independent of density, i.e. keep a constant value.

The behaviour of I_{max} *vs.* density along with fitting curves, for the considered chemical elements characterizing the investigated mixtures, are shown in Figs. 7 and 8. Experimental data have been fitted by the following double exponential decay curve:

$$y(x) = y_0 + A_1 \exp(-\frac{x - x_0}{t_1}) + A_2 \exp(-\frac{x - x_0}{t_2}) \quad (3)$$

In particular, Fig. 6a and 6b report the I_{max} values in the density range of the Y-B and Y-R mixtures (from 2.92 g cm^{-3} for the 10% Y–90% B up to 7.92 g cm^{-3} for the 10% Y–90% R) for Pb and Sn, respectively. It is worth pointing out that, since all XRF measurements of mixtures containing lead-tin yellow have been acquired with the same experimental parameters (see Experimental section for details) all I_{max} values are plotted in the same graph.

Both plots show a steeply decreasing of I_{max} as mixture density increases up to the value of 6.60 g cm^{-3}, then a plateau region, corresponding to the density values of Y-R mixtures, is reached. On the basis of the above considerations, the achievement of constant I_{max} values is to be understood as equivalent to a non-dependence of the XRF signal on the matrix density. This evidence confirms the linear calibration curves obtained for Pb and Sn in the Y-R mixtures.

Similar considerations can be made on the behaviour of I_{max} for Hg in R-B and R-Y mixtures, shown in Fig. 8a and b, respectively. Despite the different measurement parameters used for the XRF acquisitions (Panel 8a: 25 kV and 1300 μA; Panel 8b: 40 kV and 700 μA, see Experimental section for details), it is possible to find a similar behaviour with a plateau region in the 6.60–8.20 g cm^{-3} density range.

Unfortunately, due to the low efficiency of our instrumental apparatus in the detection of the light elements (such as Al and Si) components of the blue pigment, I_{max} data obtained for these two elements can only be evaluated by a qualitative point of view. However, also in this case, a dependence of I_{max} on density appears to be more noticeable in the density range of 2.40–4.50 g cm^{-3} (Fig. 8, panels c, d, e and f). This means that XRF measurements of both B-Y and B-R mixtures are affected by density changes, and all elements constituting these mixtures, as expected, cannot show a linear calibration curve.

In order to validate both the measurement and the fitting procedures, concentration values have been calculated via inverse prediction for some *ad hoc* prepared mixtures (Table 2). In the case of linear fitting, the ≅ 95% confidence ranges for concentrations, calculated by inverse prediction [44], are also reported for Pb, Hg and Sn in the R-Y mixtures.

The concentration values obtained from the fitting curves are in good agreement with the expected ones, confirming the reliability of measurements and statistical procedures. The evaluation of the behaviour of I_{max} *vs.* the mixture density suggests that, only for the linear calibration curves, it is possible to use the fitting obtained for Hg, Pb and Sn in order to gather quantitative data of these elements in matrices of density comparable to the one of the mixtures here investigated.

5. Conclusions

This work is focused on the elemental quantitative characterization of three binary mixtures obtained by varying the weight fractions of the constituting pigments. In particular, the study has concerned, after an appropriate characterization of the samples used for that purpose, the analysis of binary mixtures of cinnabar, lead-tin yellow and lapis lazuli by means of X-ray fluorescence portable spectrometer. XRF spectra for both pure pigments and mixtures obtained by varying the weight fraction in 10% step have been acquired. Net peak areas for the characteristic elements have been used to build calibration curves in order to perform inverse prediction of concentration. The outcomes highlight the different behaviour of the calibration curves with respect to the different densities of the pigments constituting the binary mixtures. Indeed, only mixtures of pigments with comparable density exhibit a linear behaviour for the net peak areas *vs.* the weight fraction. In mixtures of pigments with different densities, the slope of the net calibration curve decreases with the weight fraction of the heavy pigment, due to the increasing of the sample density. These findings, associated with those from others non-invasive methodologies, can be considered particularly useful for the recognition of weight percentage of pigments constituent an unknown painting mixture. Moreover, they provide valuable information for the establishment of a preliminary database of the chromatic palette commonly used by artists, and then useful in conservation and restoration programs.

Work in progress is to study the quantitative analytical response of measurements performed on more complex matrix and to evaluate the influences of the binding agents used for the realization of the pictorial materials.

Acknowledgements

The authors would like to thank Mr. Marcello Mirabello for the technical support.

References

[1] P.A. Lewis, Colorants: organic and inorganic pigments, in Azimuth, in: K. Nassau (Ed.), in: Color for Science, Art and technology, 1, Elsevier, Amsterdam, 1998, pp. 283–312.
[2] R. Klockenkämper, A. von Bohlen, L. Moens, Analysis of pigments and inks on oil paintings and historical manuscripts using total reflection X-ray fluorescence spectrometry, X-Ray Spectrom 29 (2000) 119–129.
[3] S. Bruni, F. Cariati, F. Casadio, L. Toniolo, Spectrochimical characterization by micro–FTIR spectroscopy of blue pigments in different polychrome works of art, Vibr. Spectro. 20 (1999) 1525.
[4] R.J.H. Clark, Pigment identification by spectroscopic means: an art/science interface, C. R. Chem. 5 (2002) 7–20.
[5] M. Sawczak, A. Kamińska, G. Rabczuk, M. Ferretti, R. Jendrzejewski, G. Śliwiński, Complementary use of the Raman and XRF techniques for non-destructive analysis of historical paint layers, Appl. Surf. Sci. 255 (2009) 5542–5545.
[6] K. Trentelman, M. Bouchard, M. Ganio, C. Namowicz, C. Schmidt Patterson, M. Walton, The examination of works of art using in situ XRF line and area scans, X-Ray Spectrom. 39 (2010) 159–166.
[7] M.F. Alberghina, R. Barraco, M. Brai, M.P. Casaletto, G.M. Ingo, M. Marrale, D. Policarpo, T. Schillaci, L. Tranchina, Degradation study of XVIII century graffiti on the walls of Chiaramonte Palace (Palermo, Italy), Appl. Phys. A 100 (2010) 953–963.
[8] M. Brai, M.P. Casaletto, G. Gennaro, M. Marrale, T. Schillaci, L. Tranchina, Degradation of stone materials in the archaeological context of the Greek–Roman Theatre in Taormina (Sicily, Italy), Appl. Phys. A 100 (2010) 945–951.
[9] P. Vandenabeele, R. Garcia-Moreno, F. Mathis, K. Leterme, E. Van Eslande, F.P. Hocquet, S. Rakkaa, D. Laboury, L. Moens, D. Strivay, M. Hartwing, Multidisciplinary investigation of the tomb of Menna (TT69), Theban Necropolis, Egypt, Spectrochim. Acta Part A 73 (2009) 546–552.
[10] L.D. Glinsman, The practical application of air-path X-ray fluorescence spectrometry in the analysis of museum objects, Rev. Conserv. 6 (2005) 3–17.
[11] C. Colombo, S. Bracci, C. Conti, M. Greco, M. Realini, Non-invasive approach in the study of polychrome terracotta sculptures: employment of the portable XRF to investigate complex stratigraphy, X-Ray Spectrom. 40 (2011) 273–279.
[12] A. Križnar, V. Muñoz, F. de la Paz, M.A. Respaldiza, M. Vega, Portable XRF study of pigments applied in Juan Hispalense's 15th century panel painting, X-Ray Spectrom. 40 (2011) 96–100.

[13] S. Pessanha, A. Guilherme, M.L. Carvalho, Comparison of matrix effects on portable and stationary XRF spectrometers for cultural heritage samples, Appl. Phys. A 97 (2009) 497–505.
[14] J.L. Ruvalcaba Sil, D. Ramírez Miranda, V. Aguilar Melo, F. Picazo, SANDRA: a portable XRF system for the study of Mexican cultural heritage, X-Ray Spectrom. 39 (2010) 338–345.
[15] A. Migliori, P. Bonanni, L. Carraresi, N. Grassi, P.A. Mandò, A novel portable XRF spectrometer with range of detection extended to low-Z elements, X-Ray Spectrom. 40 (2011) 107–112.
[16] M.F. Alberghina, R. Barraco, M. Brai, T. Schillaci, L. Tranchina, Comparison of LIBS and μ-XRF measurements on bronze alloys for monitoring plasma effects, Spectrochim. Acta B 66 (2011) 129–137.
[17] B. Hochleitner, V. Desnica, M. Mantler, M. Schreiner, Historical pigments: a collection analyzed with X-ray diffraction analysis and X-ray fluorescence analysis in order to create a database, Spectrochim. Acta B 58 (2003) 641.
[18] M. Mantler, M. Schreiner, X-ray fluorescence spectrometry in art and archaeology, X-Ray Spectrom. 29 (2000) 3–17.
[19] C. Neelmeijer, I. Brissaud, T. Calligaro, G. Demortier, A. Hautojarvi, M. Mader, L. Martinot, M. Schreiner, T. Tuurnala, G. Weber, Paintings— a challenge for XRF and PIXE analysis, X-Ray Spectrom. 29 (2000) 101–110.
[20] J.L. Ferrero, C. Roldàn, D. Juanes, E. Rollano, C. Morera, Analysis of pigment from Spanish works of art using a portable EDXRF spectrometer, X-Ray Spectrom. 31 (2002) 441–447.
[21] G. Van Der Snickt, W. De Nolf, B. Vekemans, K. Janssens, μ-XRF/μ-RS vs. SR μ-XRD for pigment identification in illuminated manuscripts, Appl. Phys. A 92 (2008) 59–68.
[22] M.L. Franquelo, A. Duran, J. Castaing, D. Arquillo, J.L. Perez-Rodriguez, XRF, XRD and spectroscopic techniques for revealing the composition and structure of paint layers on polychrome sculptures after multiple restorations, Talanta 89 (2012) 462–469.
[23] L. Burgio, R.J.H. Clark, R. Hark, Raman microscopy and X-ray fluorescence analysis of pigments on medieval and Renaissance Italian manuscript cuttings, www.pnas.org/cgi/doi/10.1073/pnas.0914797107
[24] A. Deneckere, W. Schudel, M. Van Bos, H. Wouters, A. Bergmans, P. Vandenabeele, L. Moens, In situ investigations of vault paintings in the Antwerp cathedral, Spectrochim. Acta Part A 75 (2010) 511–519.
[25] K. Trentelman, M. Bouchard, M. Ganio, C. Namowicz, C. Schmidt Patterson, M. Walton, The examination of works of art using in situ XRF line and area scans, X-Ray Spectrom 39 (2010) 159–166.
[26] R. Mayer, The Artist's Handbook of materials and techniques, Viking, NYC (USA), 1991, ISBN 0-670- 83701-6.
[27] http://www.kremer-pigmente.com/media/files_public/10620e.pdf
[28] K. Wehlte, The materials and techniques of painting, Kremer Pigments, Inc, NYC (USA), 2001, ISBN 0-9712176-0-2.
[29] M. Doerner, The materials of the artist and their use in painting, ISBN 0-15-657716-X.
[30] A. Re, A. Lo Giudice, D. Angelici, S. Calusi, L. Giuntini, M. Massi, G. Pratesi, Lapis lazuli provenance study by means of micro-PIXE, Nucl. Instr. Meth. B 269 (2011) 2373–2377.
[31] H. Kühn, Lead-tin yellow, Stud. Conserv. 13 (1968) 7–33.
[32] M. Heck, T. Rehren, P. Hoffmann, The production of lead-tin yellow at Merovingian Schleitheim (Switzerland), Archaeometry 45 (2003) 33–44.
[33] http://www.kremer-pigmente.com/media/files_public/10100e.pdf
[34] http://kremer-pigmente.de/it
[35] J. Itten, L'arte del colore, Il Saggiatore, Milano (Italy), 2007.
[36] H. Bronk, S. Röhrs, A. Bjeoumikhov, N. Langhoff, J. Schmalz, R. Wedell, H.E. Gorny, A. Herold, U. Waldschläger, ArtTAX–a new mobile spectrometer for energy-dispersive micro X-ray fluorescence spectrometry on art and archaeological objects, Fresenius J. Anal. Chem. 371 (2001) 307–316.
[37] G. Burrafato, M. Calabrese, A. Cosentino, A.M. Gueli, S.O. Troja, A. Zuccarello, ColoRaman project: Raman and fluorescence spectroscopy of oil, tempera and fresco paint pigments, J. Raman Spectrosc. 35 (2004) 879–886.
[38] L. Burgio, R.J.H. Clark, Library of FT-Raman spectra of pigments, minerals, pigment media and varnishes, and supplement to existing library of Raman spectra of pigments with visible excitation, Spectrochim. Acta Part A 57 (2001) 1491–1521.
[39] I.M. Bell, Robin J.H. Clark, P.J. Gibbs, Raman spectroscopy library of natural and synthetic pigments (pre-1850 A.D.), Spectrochim. Acta Part A 53 (1997) 2159–2179.
[40] I.M. Catalano, A. Genga, C. Laganara, R. Laviano, A. Mangone, D. Marano, A. Traini, Lapis lazuli usage for blue decoration of polychrome painted glazed pottery: a recurrent technology during the Middle Ages in Apulia (Southern Italy), J. Archaeol. Sci. 34 (2007) 503–511.
[41] P.J. Jin, W. Huang, J. Wang, G. Zhao, X.L. Wang, The identification of the pigments used to paint statues of Feixiange Cliff in China in late 19th century by micro-Raman spectroscopy and scanning electron microscopy/energy dispersive X-ray analysis, J. Mol. Struct. 983 (2010) 22–26.
[42] M. Bertucci, L. Bonizzoni, N. Ludwig, M. Milazzo, A new model for x-ray fluorescence autoabsorption analysis of pigment layers, X-Ray Spectrom. 39 (2010) 135–141.
[43] G.E. Gigante, R. Cesareo, Non destructive analysis of ancient metal alloys by in situ EDXRF transportable equipment, Radiat. Phys. Chem. 51 (1998) 689–700.
[44] F.A. Graybill, Theory and application of the linear model, Duxbury Press, Belmont (USA), 1976, pp. 280–3.